Configurations of the Flow Induced by a Fan Impeller without Casing

Lecturer PhD Eng. **Andrei DRAGOMIRESCU**[1]

[1] University Politehnica of Bucharest, Department of Hydraulics, Hydraulic Machinery and Environmental Engineering, andrei.dragomirescu@upb.ro

Abstract: *This paper presents a study of the turbulent, compressible air flow induced by a fan impeller without scroll casing. The equations governing the flow – continuity equation, momentum equations, energy equation and the equation of state – were solved numerically using the finite volume method. The Reynolds Stress Model was used to provide the closure equations. Different simulations were made by changing the overpressure imposed as boundary condition at the outflow. The overpressure was varied stepwise between the choke limit and the limit corresponding to reversed flow. Despite the symmetry of geometry and boundary conditions, the results obtained indicate the appearance of non-axisymmetrical solutions. Moreover, two bifurcating solutions were obtained at certain operating points. These solutions are characterized by two and, respectively, three dominant directions of the flow outside the impeller. By dominant directions we denote regions where the velocity is higher than in neighboring areas at the same radius. Based on the results, a bifurcation diagram is plotted. The bifurcating solutions lead to different values of the average mass flow rate delivered by the impeller for the same outflow pressure. This could offer an explanation for the hysteresis of the characteristic curves of some pneumatic turbomachines. Moreover, the dominant directions extend inside the impeller and cause time-periodic pressure pulsations on the blade, which could be an additional explanation for the vibrations and noise in pneumatic turbomachines.*

Keywords*: bifurcating solutions, compressible flow, flow configurations, free impeller, high pressure fan*

1. Introduction

High pressure fans are fans that, considering the classifications in ISO 13349 [1], have compression rations between 1.1 and 1.3 when they pump air having a density of 1.2 kg/m^3. The EUROVENT norms [2] define different limits and, according to them, high pressure fans have compression ratios between 1.036 and 1.3. The compressible turbulent gas flows (usually air flows) induced by impellers of high pressure fans are governed by the equation of state and several partial differential equations: continuity equation, momentum equations, and energy equation. To these, the closure equations corresponding to the turbulence model chosen to study the flow should be added. Due to the continuous movement of the fan impeller, the gas flow is inherently unsteady, so that the governing partial differential equations can be written in the following condensed form:

$$\frac{\mathrm{d}\mathbf{U}}{\mathrm{d}t} = \mathbf{F}(\boldsymbol{\mu}, \mathbf{U}), \tag{1}$$

with the initial value

$$\mathbf{U}(0) = \mathbf{U}_0 \tag{2}$$

and associated boundary conditions. In the above equations $\mathbf{U}$ is the vector of flow variables (velocity components, pressure, temperature, density, turbulent variables), $\mathbf{F}$ is a vector function whose components are functions of the components of $\mathbf{U}$, and $\boldsymbol{\mu}$ is a vector of parameters (gas viscosity, coefficient of thermal conductivity, etc.). A solution to which equation (1) evolves after the transient effects associated with the initial values (2) have diminished is called *asymptotic solution*. It should be mentioned here that $\mathbf{U} = \mathbf{0}$ cannot be a solution of the problem, since $\mathbf{U} \neq \mathbf{0}$ is forced by nonzero forcing data embedded in $\mathbf{F}(\boldsymbol{\mu}, \mathbf{U})$, and, if applicable, in the boundary conditions. Examples of nonzero forcing data are the pressure force per unit mass, $\nabla p/\varrho$, and, in a non-inertial reference frame attached to the impeller, the centrifugal force per unit mass, $\boldsymbol{\omega} \times (\boldsymbol{\omega} \times \mathbf{r})$, where ϱ is the gas density, vector $\boldsymbol{\omega}$ is the angular velocity of the impeller, and $\mathbf{r}$ is the position vector. Among the possible asymptotic solutions of the autonomous problem formulated above there are (i) steady solutions and (ii) T-periodic solutions of the form $\mathbf{U}(t) = \mathbf{U}(t + T)$. Asymptotic solutions

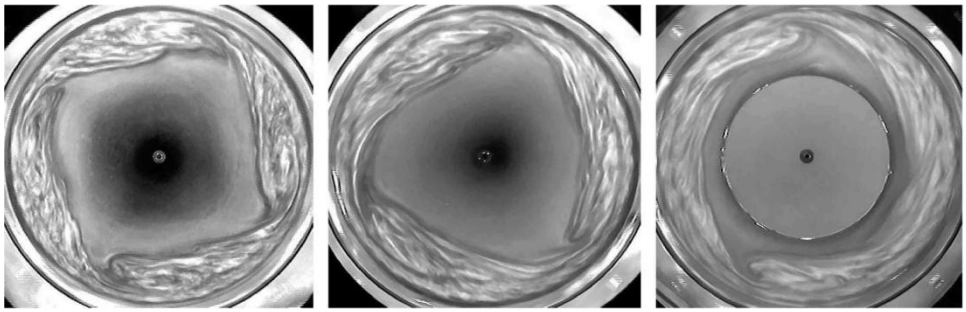

Fig. 1. Flow configurations induced by a disc rotating inside a casing, obtained experimentally by Poncet and Chauve [8]

which form intersecting branches in a suitable space of functions are called *bifurcating solutions*. It is said that one asymptotic solution bifurcates from another at $\boldsymbol{\mu} = \boldsymbol{\mu}_0$ if there are two distinct asymptotic solutions $\mathbf{U}^1(\boldsymbol{\mu}, t)$ and $\mathbf{U}^2(\boldsymbol{\mu}, t)$, continuous in $\boldsymbol{\mu}$, such that $\mathbf{U}^1(\boldsymbol{\mu}_0, t) = \mathbf{U}^2(\boldsymbol{\mu}_0, t)$. One work, in which the bifurcation theory is extensively treated, is that of Ioos and Joseph [3].
An important characteristic of bifurcation is the appearance of solutions that can break the symmetry pattern of the forcing data, should this symmetry exists. Thus, non-symmetrical solutions are possible even when the geometry and the boundary conditions are symmetrical.
It is often true that a necessary condition for bifurcation is the instability of the asymptotic solution to small disturbances. In a real flow, disturbances are usually small deviations in the symmetry of the geometry due to manufacturing imperfections, slight changes in the upstream or downstream flow conditions, etc. In a numerical simulation, disturbances can be introduced by the inherent numerical errors.
Bifurcating solutions were found experimentally and numerically even in cases of simple flows, like those through symmetrical sudden expansions [4, 5], through a symmetrical channel with a sudden expansion and a sudden contraction [6], or through a lid driven cavity with throughflow [7]. More recently, Poncet and Chauve [8] identified experimentally different configurations, without axial symmetry, of the flow induced by a rotating disc enclosed by a fixed cylindrical shroud. Central hubs having different radii were attached to the disk. Above a certain threshold, the flow shows different modes characterized by sharp-cornered polygonal patterns with m vortices. The number of vortices changes as the rotational Reynolds number, Re, increases and shows a noticeably hysteresis when Re decreases. Three modes observed by Poncet and Chauve, with 2, 3, and 4 vortices, are presented in Figure 1 for subsequent comparisons. Ciocanea [9] investigated numerically the fluid motion induced by a rotating disk inside a vessel and found flow configurations with different numbers of inner vortices depending on the Reynolds number calculated based on disk radius.
This paper investigates another type of rotational flow and its instabilities. It is the compressible turbulent air flow induced by a free impeller, i.e. an impeller without scroll casing, of a high pressure fan. The study was performed by means of numerical simulations. In the following, the problem is formulated in terms of geometry, flow equations, fluid parameters and numerical algorithms. The results are then presented and discussed and conclusions are drawn.

2. Problem description

The study was performed for the impeller of a high pressure fan designed for a rated compression ratio of $\tau = 1.3$ and a rotational speed of $5000\ \mathrm{rpm}$ to which the angular velocity $\omega = 526.6\ \mathrm{rad/s}$ and the rotational frequency $f = 83.33\ \mathrm{Hz}$ correspond. The design was based on a method proposed by Pfleiderer and Petermann [10]. In many cases, in order to keep the geometry of the machine as simple as possible, so that the manufacturing process is simplified and the cost is reduced, fan impellers have a constant width from inlet to outlet. For this reason we chose to use a two-dimensional geometry in our study. The computational domain consists of the impeller and two annular zones placed inside and outside the impeller. A sketch of a part of the computational domain, comprising the impeller, is presented in Figure 2. The impeller rotates counter-clockwise. The diameter at impeller inlet is $D_1 = 330\ \mathrm{mm}$, while at outlet the diameter is $D_2 = 660\ \mathrm{mm}$. The

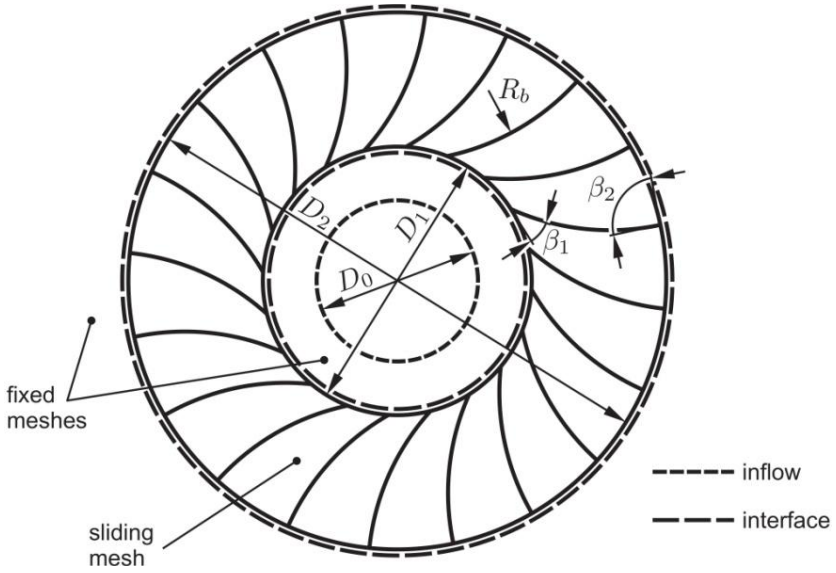

Fig. 2. Impeller geometry and configuration of the computational domain

impeller has 20 blades shaped as circular arcs of radius $R_b = 296\ \mathrm{mm}$ and having the angles $\beta_1 = 33.5°$ at inlet and $\beta_2 = 90°$ at outlet. For the imposed rotational speed and the chosen number of blades, the blade passing frequency is $f_b = 1666.7\ \mathrm{Hz}$.

The inflow boundary is situated at diameter $D_0 = 0.6D_1 = 198\ \mathrm{mm}$, while the outflow boundary lies at diameter $D_3 = 3D_2 = 2040\ \mathrm{mm}$. For the sake of clarity, diameter D_3 is not visible in Figure 2. The working fluid is air considered to be a perfect gas.

Both the turbulence and the rotational movement of the impeller render the flow unsteady. Turbulence was treated using a second order closure model, namely the Reynolds Stress Model. The reason for this choice, instead of a simpler, two equations model, is that second order closure models are designed to handle effects that cannot be caught by two equations turbulence models. Such effects are streamline curvature, sudden changes in strain rate, and secondary motion, which are likely to appear in the flow under study. In the Reynolds Stress Model the turbulent stresses are not modeled but solved, one additional transport equation being added for each turbulent stress [11].

The equations governing the unsteady turbulent compressible flow – continuity equation, momentum equations, energy equation, transport equations for turbulent quantities, and equation of state – were solved numerically by means of the finite volume method using the coupled solver in implicit formulation implemented in the commercial code Ansys Fluent. The continuity, momentum and energy equations were discretized using a second order upwind scheme, while the Reynolds stresses were discretized with a first order upwind scheme. The temporal discretization of the coupled equations was accomplished by a second order implicit time-marching scheme.

The reference pressure and the reference absolute temperature were chosen as $p_0 = 10^5\ \mathrm{Pa}$ and $T_0 = 300\ \mathrm{K}$, respectively. The required properties of air – dynamic viscosity, specific heat at constant pressure, and coefficient of thermal conductivity – were input as piece-wise linear functions of temperature using data found in literature [11]. As boundary conditions, the relative total pressure $p_{t_0} = 0\ \mathrm{Pa}$ and the absolute temperature $T_0 = 300\ \mathrm{K}$ were set at inflow. The no-slip condition was imposed on the blades. Simulations were performed for relative static pressures at outflow, p_r, ranging from $16000\ \mathrm{Pa}$ to $34000\ \mathrm{Pa}$.

The first simulation was performed for an outflow pressure of $20000\ \mathrm{Pa}$. The initial guess for this simulation was obtained through auxiliary computations, in which the angular velocity of the impeller and the outflow static pressure were increased stepwise, in a coupled manner, starting from values close to zero, until the angular velocity reached the desired value of $523.6\ \mathrm{rad/s}$ at an outflow pressure of $20000\ \mathrm{Pa}$. After that, the solution of the last time step of each simulation was used as initial guess for the next simulation. For each new simulation the outflow static pressure was increased or decreased, as appropriate, by $1000\ \mathrm{Pa}$. At each value of the outflow static pressure the simulations were advanced in time with the time step $\Delta t = 0.00015\ s$ until a

stabilization of the mass flow rate delivered by the impeller around an average value was observed for at least 40 revolutions of the impeller (3200 time steps).
As convergence criterion the drop of all scaled residuals by at least three orders of magnitude at each time step was imposed. The residuals were scaled by dividing them to the highest residual obtained in the first five iterations of the first auxiliary simulation.
Simulations were attempted also for outflow static pressures outside the range $16000 \ldots 34000\ \mathrm{Pa}$, but the results suggested that pressures below $16000\ \mathrm{Pa}$ lead to choke, while pressures above $34000\ \mathrm{Pa}$ cause a reversed flow through the impeller.

3. Results and discussion

The first results, obtained for $p_r = 20000\ \mathrm{Pa}$, indicate that outside the impeller the flow is not axisymmetrical, as expected, but it shows three regions of higher velocity. We will denote further these regions as dominant flow directions. Figure 3 shows contours of absolute velocity and streamlines plotted outside the impeller, which make evident the dominant flow directions. It can be seen that the three directions are practically equally spaced at angles of $120°$, the flow possessing a three-fold rotational symmetry with respect to impeller axis.
An image of an axisymmetrical flow, which could be induced by the impeller under study, can be obtained by means of the potential flow theory. The usage of considerations derived from this theory when designing turbomachines remains a common practice. If the flow outside the impeller is accepted to be potential and incompressible, then this flow can be regarded as a superposition of a source of volumetric flow rate Q and a potential vortex of circulation Γ, which rotates counter-clockwise, as the impeller does. The streamlines of such a flow are logarithmic spirals, which in polar coordinates (r, θ) have the equation

$$r = A\mathrm{e}^{(Q/\Gamma)\theta}, \tag{3}$$

where A is a constant whose value identifies a specific streamline in the family of streamlines. For a given streamline, the constant A can be easily computed if the coordinates (r, θ) of a point of the streamline are known. Both the flow rate Q and the circulation Γ can be computed using the results of the simulations. The flow rate should be equal to that pumped by the impeller and, at a particular diameter D, it can be computed with the formula

$$Q = \int_0^{\pi D} v_r\,\mathrm{d}s\,, \tag{4}$$

where v_r is the radial velocity obtained from simulations at diameter D and s is the coordinate along the circular path of diameter D.

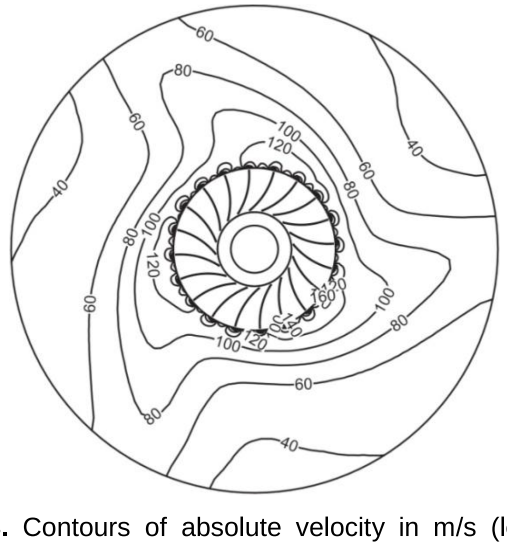

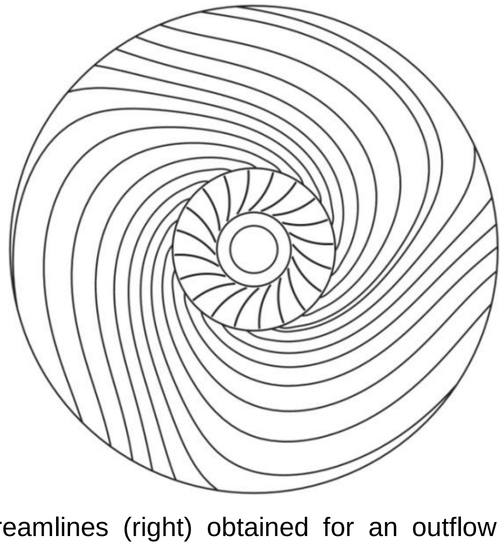

Fig. 3. Contours of absolute velocity in m/s (left) and streamlines (right) obtained for an outflow static pressure $p_r = 20000\ \mathrm{Pa}$, showing three dominant flow directions

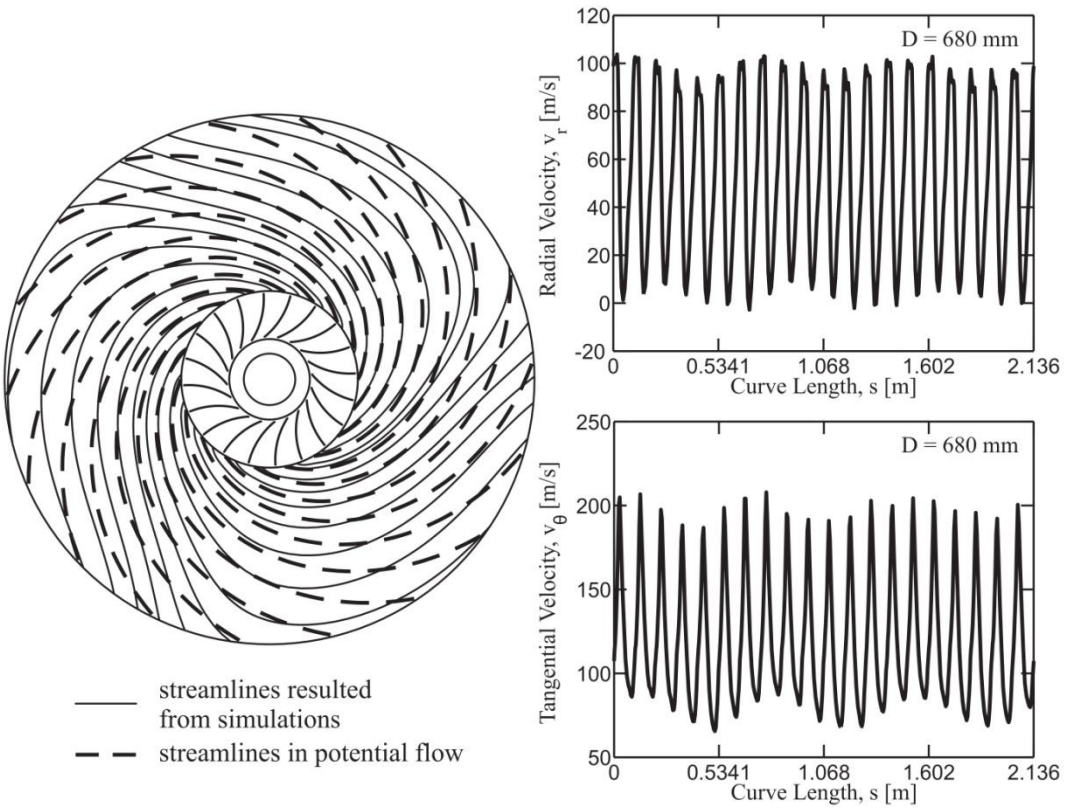

Fig. 4. Comparison between streamlines resulted from simulations at $p_r = 20000\ \mathrm{Pa}$ and streamlines computed based on potential flow theory (left); velocity distributions resulted from simulations and used to compute the volume flow rate and the velocity circulation at a diameter of $680\ \mathrm{mm}$ (right)

The circulation is given by the formula

$$\Gamma = \int_0^{\pi D} v_\theta \, \mathrm{d}s \,, \tag{5}$$

where v_θ is the tangential velocity obtained from simulations at diameter D. The flow rate and the circulation were computed at the interface between impeller zone and outflow zone. This interface is located at diameter $D = 680\ \mathrm{mm}$, very close to impeller. By integrating the velocity distributions resulted from simulations at $p_r = 20000\ \mathrm{Pa}$ and presented in Figure 4, $Q \approx 110.9\ \mathrm{m^3/s \cdot m}$ and $\Gamma \approx 255.6\ \mathrm{m^2/s}$ were obtained. With these values of Q and Γ, 20 equaly spaced streamlines of the potential flow were computed. These analitical streamlines are compared in Figure 4 with streamlines obtained numerically. It can be noticed that close to impeler a very good agreement exists between the two families of streamlines.

Subsequent simulations that were continued from the configuration with three dominant directions obtained at $p_r = 20000\ \mathrm{Pa}$ showed that the number of dominant directions, i.e. three directions, remained unchanged for p_r values in the range $16000 \ldots 24000\ \mathrm{Pa}$.

The image of the flow induced by the impeller changed after the outflow static pressure was increased from $24000\ \mathrm{Pa}$ to $25000\ \mathrm{Pa}$ and the flow rate became stable: the three dominant directions were replaced by only two dominant directions. As the outflow static pressure was further increased, this flow configuration remained unchanged up to $p_r = 29000\ \mathrm{Pa}$. The flow configuration with two dominant directions is depicted in Figure 5 by a contour plot of the velocity magnitude and streamlines obtained for $p_r = 28000\ \mathrm{Pa}$. With the two dominant directions spaced at $180°$, the flow possesses a two-fold rotational symmetry with respect to impeller axis.

For values of p_r between $30000\ \mathrm{Pa}$ and $32000\ \mathrm{Pa}$ the three dominant directions reappeared (Fig. 6). Finally, close to the limit of reversed flow, at $p_r = 33000\ \mathrm{Pa}$ and $p_r = 34000\ \mathrm{Pa}$, the results indicated again flow configurations with only two dominant directions (Fig. 7).

The first set of results described above indicate flow configurations with either three or two

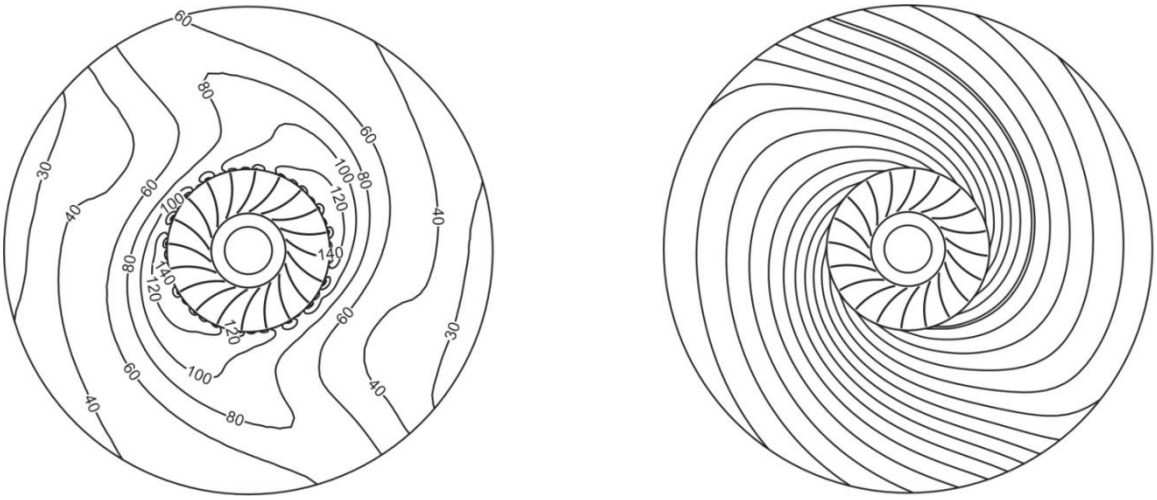

Fig. 5. Contours of absolute velocity in m/s (left) and streamlines (right) obtained for an outflow static pressure $p_r = 28000$ Pa, showing two dominant flow directions

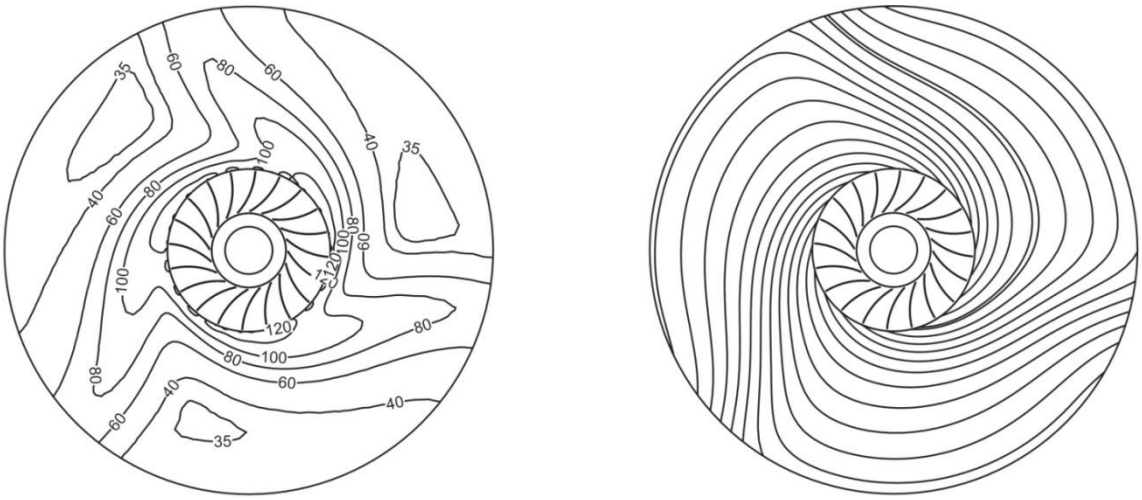

Fig. 6. Contours of absolute velocity in m/s (left) and streamlines (right) obtained for an outflow static pressure $p_r = 30000$ Pa, showing (again) three dominant flow directions

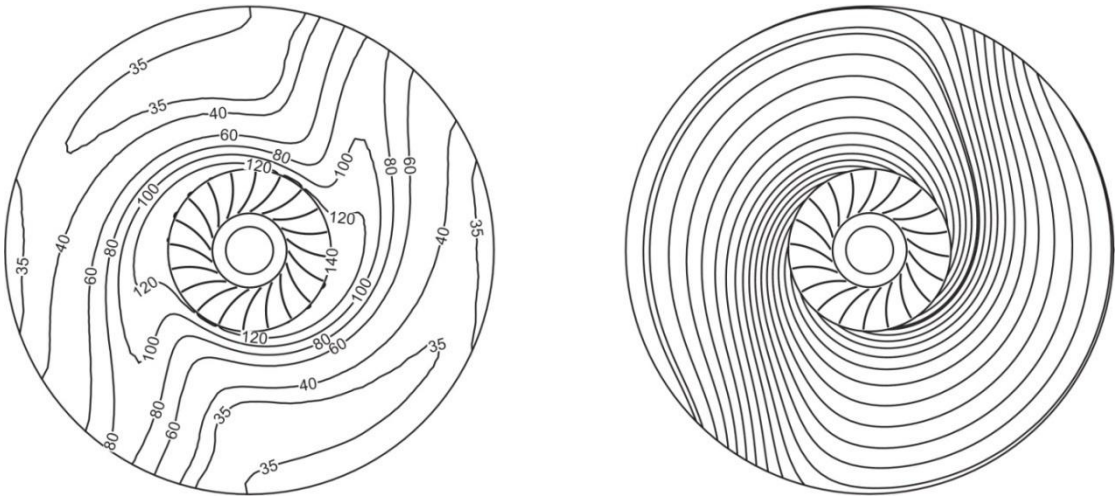

Fig. 7. Contours of absolute velocity in m/s (left) and streamlines (right) obtained for an outflow static pressure $p_r = 34000$ Pa, showing two dominant flow directions

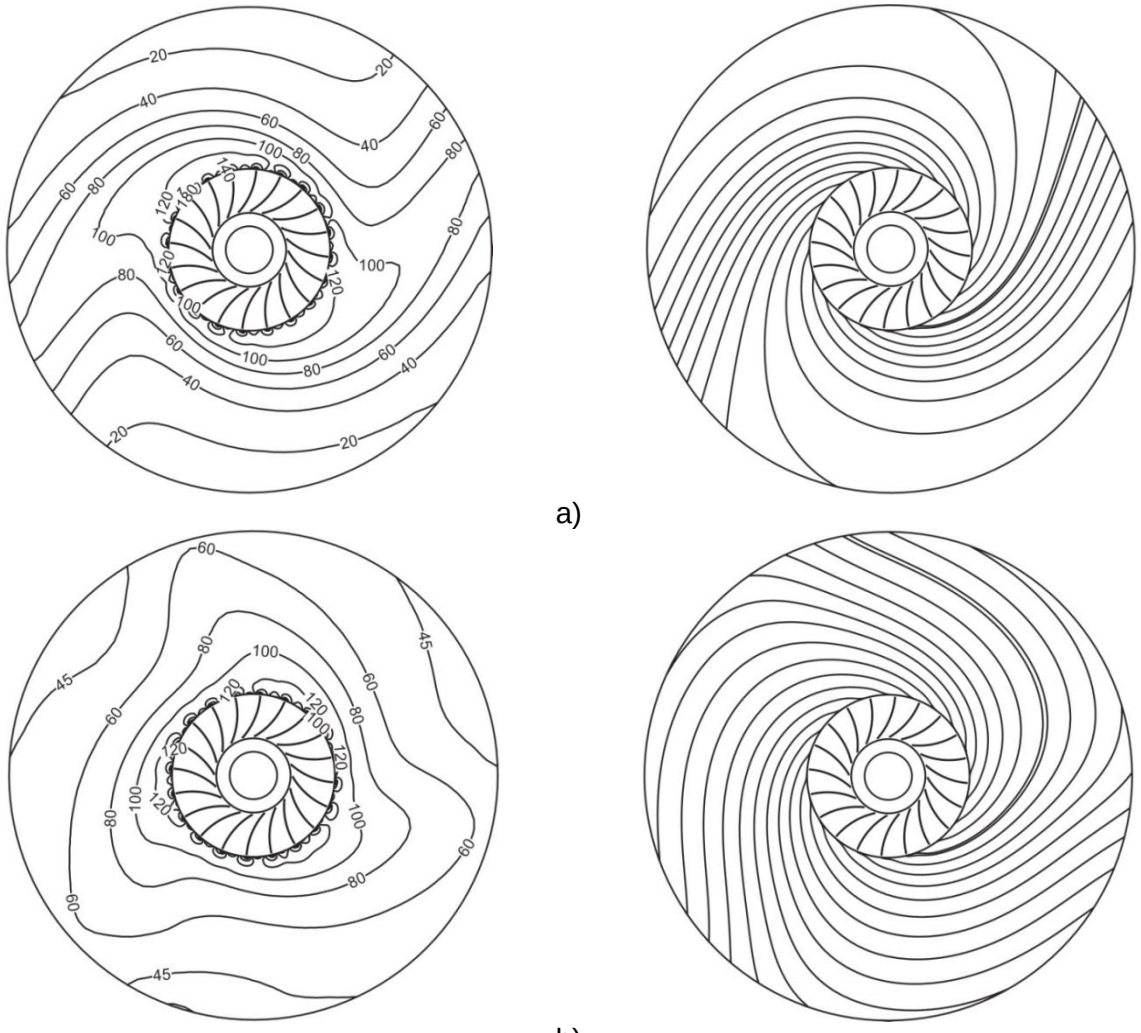

Fig. 8. Contours of absolute velocity in m/s (left) and streamlines (right) obtained for an outflow static pressure $p_r = 34000$ Pa, showing two dominant flow directions

dominant directions, depending on the working regime of the impeller, characterized by the outflow static pressure p_r. To verify these results, new simulations were started from the last solution obtained for the outflow static pressure of 34000 Pa. The new set of simulations was continued by decreasing p_r stepwise by 1000 Pa. Down to $p_r = 25000$ Pa, the new results showed no change in the flow configurations by comparison with those obtained previously. A change appeared only when p_r was decreased from 25000 Pa to 24000 Pa. Instead of observing a switch from two dominant directions to three directions, as expected based on the previous results, the flow preserved its two dominant directions down to $p_r = 16000$ Pa. In other words, when decreasing the outflow static pressure below 30000 Pa in small steps only flow configurations with two dominant directions can be obtained. Figure 8 presents for comparison contours of absolute velocity and streamlines showing two flow configurations, both obtained at the same outflow static pressure $p_r = 24000$ Pa.

A third set of results was obtained by increasing the outflow static pressure starting from the solution showing two dominant flow directions resulted for $p_r = 16000$ Pa in the second set of simulations. The flow configuration remained unchanged, with two dominant directions, up to $p_r = 29000$ Pa, it changed to three dominant directions for p_r between 30000 Pa and 32000 Pa and then back to two directions for p_r between 33000 Pa and 34000 Pa.

The fact that below $p_r = 25000$ Pa two flow configurations are possible indicates that a bifurcation point exists between $p_r = 24000$ Pa and $p_r = 25000$ Pa. The results presented above are

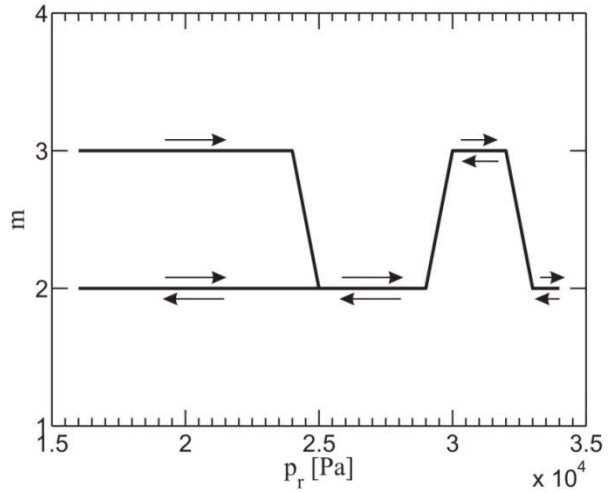

Fig. 9. Bifurcation diagram

summarized in the form of a bifurcation diagram in Figure 9. The diagram shows the number of flow directions, m, depending on the outflow static pressure p_r. According to the results, the branch corresponding to $m = 2$ can be traversed in both directions as long as the outflow static pressure changes in small steps. According to our results, if only small pressure changes are applied, close to the bifurcation point flow configurations with tree dominant directions evolve in flow configurations with two directions but flow configurations with two directions cannot evolve in flow configurations with three directions.

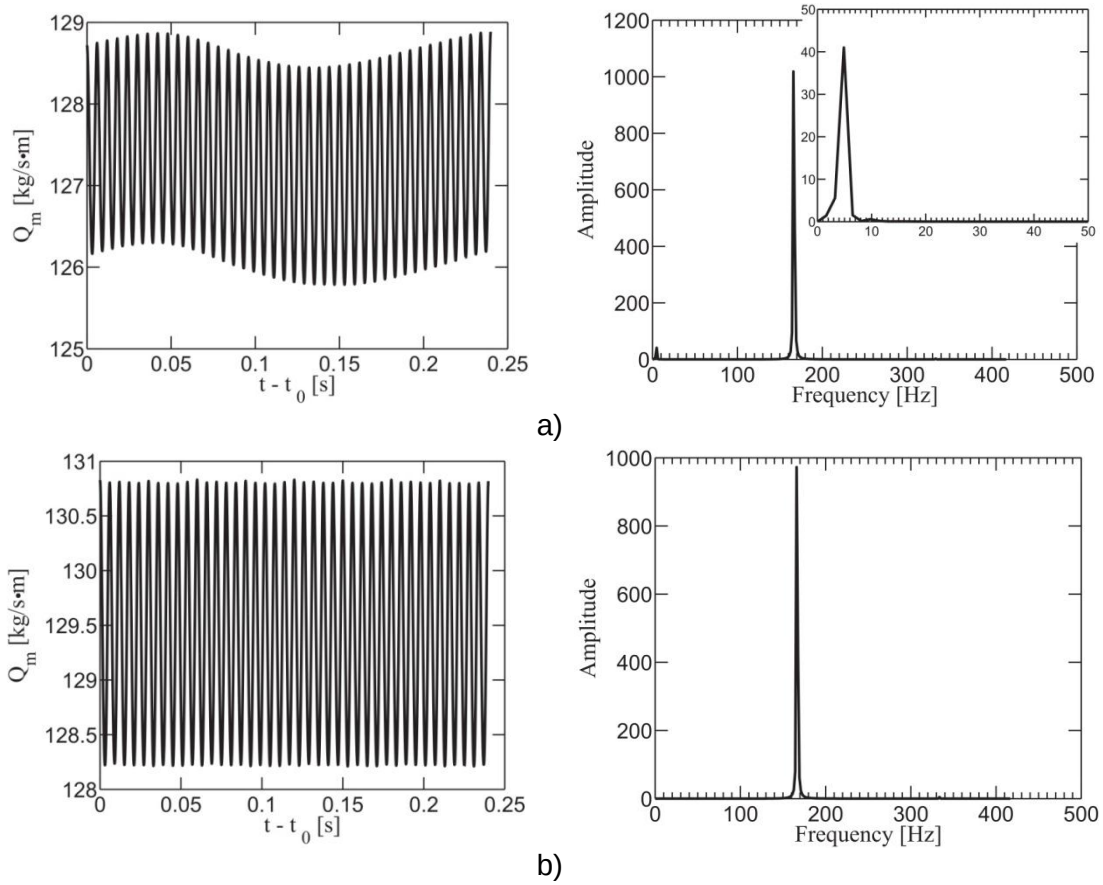

Fig. 10. Mass flow rate variations and their frequency spectra at outflow for 1600 time steps (20 full rotations) resulted at $p_r = 24000$ Pa when the flow shows: a) two dominant directions and b) three dominant directions

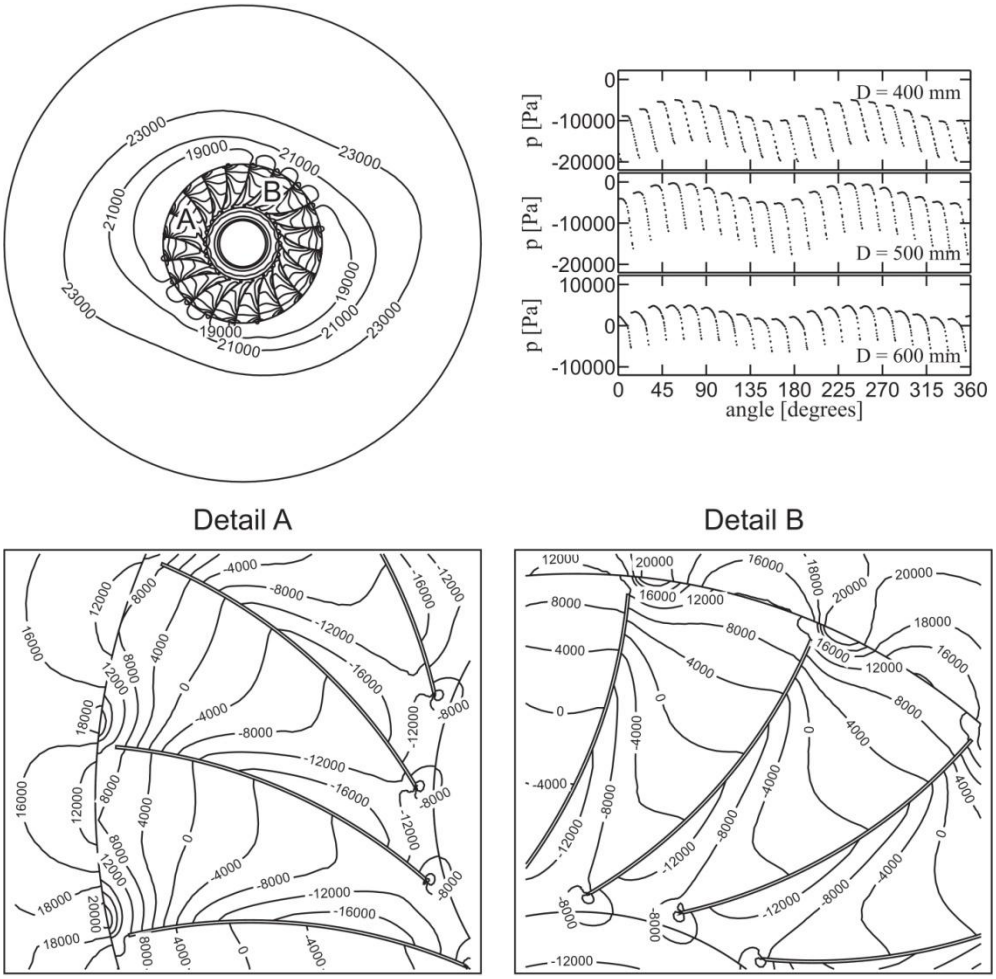

Fig. 11. Contours of static pressure in Pa and circumferential pressure variations at three diameters inside the impeller ($D = 400$ mm, $D = 500$ mm, and $D = 600$ mm) resulted at $p_r = 24000$ Pa when the flow shows two dominant directions

The evolution in time of the mass flow rate Q_m at outflow changes depending on the flow configuration. The change is depicted in Figure 10 which shows time variations of Q_m and the frequency spectra of these variations obtained for $p_r = 24000$ Pa. It can be seen that, when the flow has two dominant directions, the mass flow rate has two modes of oscillation. For three dominant directions only one mode of oscillation is evident. In both cases, the first mode of oscillations has a frequency of 166.66 Hz, which is twice the rotational frequency of the impeller. For the flow with two dominant directions, the value of the first oscillation frequency could be related to the fact that, during a full revolution of the impeller, each blade interacts twice with the dominant flow directions. However, this explanation is no more valid for the flow with three dominant directions, which makes us to assume that the flow rate oscillations are caused by a more complex mechanism which probably includes the effect of the dominant flow directions and, also, the air compressibility. Another observation is that the configuration of the flow has also an influence on the average mass flow rate delivered by the impeller. For $p_r = 24000$ Pa the value of the average flow rate equals $127.3\ \mathrm{kg/s \cdot m}$ when the flow shows two dominant directions and $129.5\ \mathrm{kg/s \cdot m}$ when the flow has three directions, the relative difference being of about 1.7%. The bifurcation of the flow solutions could, therefore, offer an explanation for the small hysteresis of the characteristic curve observed in some cases when testing pneumatic turbomachines.

It is expected that the development of dominant flow directions outside the impeller has an influence on the flow inside the impeller. Of interest is especially the pressure, since pressure pulsations are among the causes for vibrations and aerodynamically generated noise in fans. Therefore, the pressure field was examined both for the configuration with two dominant flow directions and for the configuration with three directions. The configurations are those obtained for

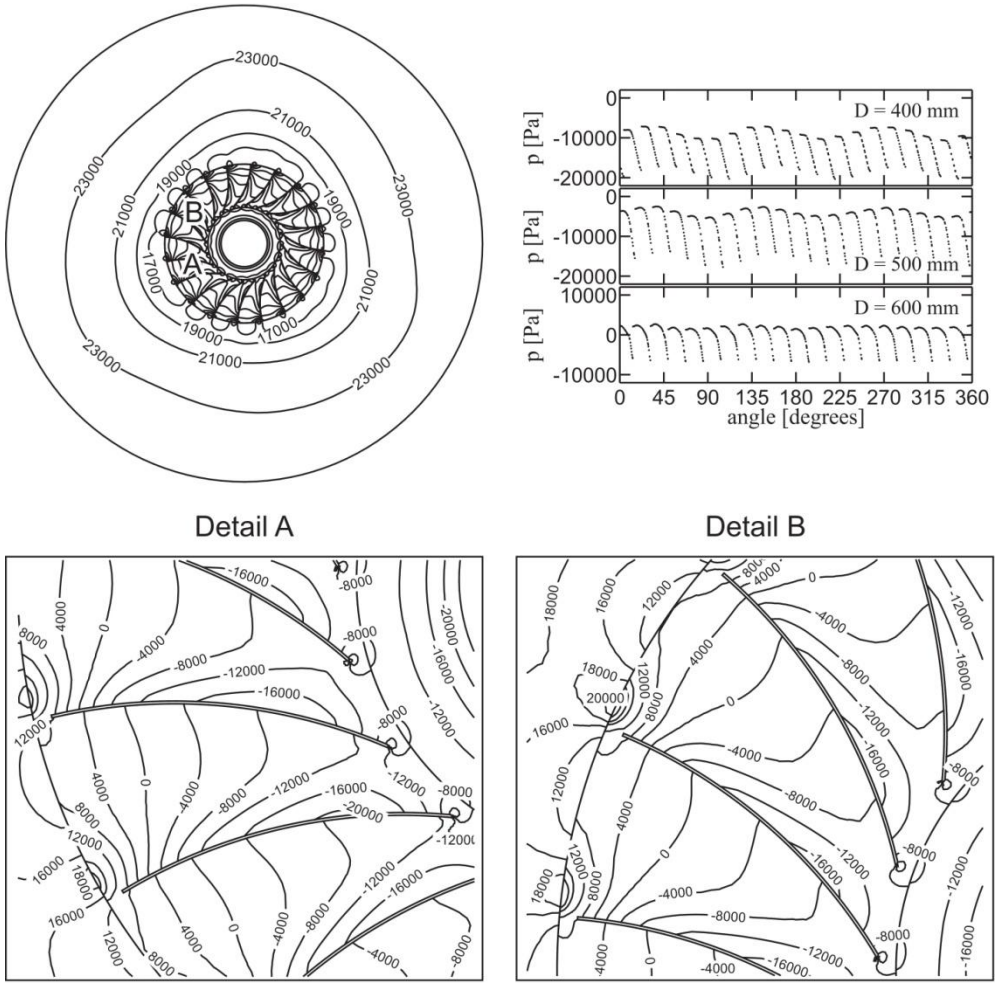

Fig. 12. Contours of static pressure in Pa and circumferential pressure variations at three diameters inside the impeller ($D = 400$ mm, $D = 500$ mm, and $D = 600$ mm) resulted at $p_r = 24000$ Pa when the flow shows three dominant directions

an outflow static pressure of 24000 Pa. Figures 11 and 12 present circumferential pressure variations inside the impeller and pressure contours plotted inside blade channels which, at a certain time moment, either are aligned with a dominant flow direction or lie between two directions. The pressure distributions on the pressure sides and on the suction sides of the blades show noticeable changes as a blade crosses a dominant direction and then moves at angular positions between two dominant directions. These changes are also made evident by the diagrams of circumferential pressure variations, which show that during a full revolution of the impeller the blades undergo pressure pulsations, the number of maxima and minima being equal to the number of dominant flow directions. This shows that the dominant flow directions do not lie only outside the impeller, but extend inside it. The flow configuration outside the impeller influences the pressure pulsations, which are of lower amplitude when the flow exhibits three dominant directions. Therefore, the flow configuration with three dominant directions could be more desirable.

4. Conclusions

In this paper the compressible turbulent flow induced by a free impeller of a high pressure fan was investigated by means of numerical simulations. According to the results obtained, the flow outside the impeller is not axisymmetrical, but possesses either two or three dominant flow directions, depending on the boundary conditions. There is a certain similarity between the flow configuration presented in this paper and those observed by Poncet and Chauve for the flow induced by a disc rotating inside a fixed shroud. In a certain range of boundary conditions the flow solutions bifurcate, both flow configurations being possible. Based on the results, a bifurcation diagram was plotted.

The time variations of the mass flow rate delivered by the impeller are visibly influenced by the flow configurations. In the range of bifurcating solutions, the values of the average mass flow rate differ depending on the flow configuration. This fact could explain, at least partly, the small hysteresis of the characteristic curves obtained when testing some pneumatic turbomachines. The dominant flow directions extend inside the impeller, causing pressure pulsation on the blades. The flow instability investigated in this paper could therefore be an additional explanation for vibrations and aerodynamically generated noise inside pneumatic turbomachines.

References

[1] ISO 13349:2010, "Fans – Vocabulary and definitions of categories", ISO, 2010;
[2] EUROVENT 1/1, "Fan Terminology", EUROVENT/CECOMAF, 1984;
[3] G. Ioos, D.D. Joseph, "Elementary stability and bifurcation theory", 2nd Edition, Springer, New York, 1990;
[4] W. Cherdron, F. Durst, J.H. Whitelaw, "Asymmetric flows and instabilities in symmetric ducts with sudden expansion", Journal of Fluid Mechanics, 84, 1978, pp. 13–31;
[5] R.M. Fearn, T. Mullin, K.A. Cliffe, "Nonlinear flow phenomena in a symmetric sudden expansion", Journal of Fluid Mechanics, 211, 1990, pp. 595–608;
[6] J. Mitzushima, Y. Shiotani, "Transitions and instabilities of flow in a symmetric channel with a suddenly expanded and contracted part", Journal of Fluid Mechanics, 434, 2001, pp. 355–369;
[7] Dragomirescu, "Flow configurations in a lid driven cavity with throughflow", University Politehnica of Bucharest Scientific Bulletin, Series D: Mechanical Engineering, 66, 2–4, 2004, pp. 137–148;
[8] S. Poncet, M.P. Chauve, "Shear-layer instability in a rotating system", Journal of Flow Visualization and Image Processing, 14, 2007, pp. 85–105;
[9] A. Ciocanea, "Numerical Study on the Fluid Motion Induced by a Rotating Disk Inside a Vessel", Hidraulica, 4, 2013, pp. 65–69;
[10] Pfleiderer, H. Petermann, "Strömungsmaschinen", 4th Edition, Springer, Berlin, 1991;
[11] T.J. Chung, Computational Fluid Dynamics, Cambridge University Press, 2002;
[12] H.D. Baehr, K. Stephan, "Wärme- und Stoffübertragung", 3rd Edition, Springer, Berlin, 1998;
[13] H.K. Versteeg, W. Malalasekera, "An Introduction to Fluid Dynamics – The Finite Volume Method", Longman Scientifical and Technical, London, 1996;
[14] F.S. Lien, M.A. Leschziner, "Assessment of Turbulent Transport Models Including Non-Linear RNG Eddy-Viscosity Formulation and Second Moment Closure", Computers and Fluids, 23, 8, 1994, pp. 983–1004;
[15] B.E. Launder, "Second-Moment Closure and Its Use in Modeling Turbulent Industrial Flows", International Journal for Numerical Methods in Fluids, 9, 1989, pp. 963–985;
[16] B.E. Launder, D.B. Spalding, "The Numerical Computation of Turbulent Flows", Computer Methods in Applied Mechanics and Engineering, 3, 1974, 269–289.